Chalcogenide Letters Vol. 19, No. 3, March 2022, p. 203 - 216

Green synthesis of ZnS nanoparticles using *allium sativum l.* extract and study of their structural, optical and electrical properties

U. S. Senapati[a,*], R. Athparia[b]
[a]*Department of Physics, Handique Girls' College, Guwahati-781001, Assam, India*
[b]*Department of Physics, Gauhati University, Guwahati-781014, Assam, India*

This work presents a simple, low-cost and environmentally friendly approach for the synthesis of zinc sulfide nanoparticles (ZnS NPs) using *Allium sativum L.* plant extract. Formation of cubic ZnS NPs is confirmed from X-ray diffraction study. Transmission electron microscopy image confirms the formation of spherical particles of average size 6.5 nm. Direct band gap energy of the NPs is found to increase from 3.87 – 4.25 eV with increasing volume of the extract. Fourier transform infrared spectroscopy analysis confirms the presence of biomolecules in the extract which are involved in the formation of ZnS NPs. The possible growth mechanism of ZnS NPs within the biopolymer matrix has been discussed. The dielectric constant of ZnS NPs is higher than the bulk ZnS. A.C. conductivity increases with increasing frequency and changes practically linearly with applied frequency. The impedance study suggests that the ZnS samples could be used as nano-tuned devices in electronics. It is found that as crystallite size decreases, d.c conductivity rises.

(Received December 28, 2021; Accepted March 18, 2022)

Keywords: Green synthesis, ZnS NPs, Dielectric constant, A.C. conductivity, Impedance, D.C. conductivity

1. Introduction

Zinc sulfide (ZnS) is a promising II-VI group semiconductor material with a wide direct band gap of 3.68 eV [1, 2]. This material has been extensively investigated due to its applications in electronic, optoelectronic and electrochemical devices [1]. ZnS nanoparticles (NPs) show distinct properties which are different from its bulk counterpart because of very high surface to volume ratio. ZnS NPs can be synthesized by using a variety of chemical and physical methods [3-7]. However, these syntheses methods are not environment friendly. Therefore, green synthesis of nanoparticles is given much attention as this process is quick and suitable for large scale production. Currently, medicinal plants are used for green synthesis of nanoparticles due to their ability to control the size and shape of nanoparticles by providing capping layers [8]. In our earlier work [9], a medicinal plant *Elaeocarpus floribundus* was successfully used for the green synthesis of ZnS NPs. Recently, Alijani et al. [10] and Tudu et al. [2] have also used medicinal plants for the same purpose. But the potential of medicinal plants as bio-capping agent for the synthesis of this technologically demanding semiconductor material is still fully not explored. In the present study a locally available medicinal plant *Allium sativum L.* (*A. sativum L.)* is used to synthesize ZnS NPs. Literature studies have shown that *A. sativum L.* is rich in alkaloids, tannis, carotenoids, saponins, phenols and flavonids [11]. These bio-constituents may be considered as potential factors for reducing and capping of nanopartcles.

* Corresponding author e-mail: udaysankargu@gmail.com
https://doi.org/10.15251/CL.2022.193.203

2. Experimental

2.1. Materials

Fresh *A. sativum L.* was purchased from the local vegetable market in Guwahati, Assam, India. $ZnCl_2$ (Merck specialties pvt. Ltd.) and Na_2S (Qualigens fine chemicals) were used as zinc and sulphur source respectively. These were of high purity and used without any further purification.

2.2. Preparation of *A. sativum L.* extract

30 g of fresh and cleaned *A. sativum L.* was crushed into fine fragments using mortar and pestle. The fine fragments were boiled in 100 ml of distilled water for 15 minutes before being filtered. The filtrate was cooled to room temperature. The resultant filtrate was stored at 4^0C till further use [12]. Figure1 shows the *A. sativum L.* and its extract.

Fig. 1. (a) Freshed A. sativum L. (b) cleaned A. sativum L.and (c) extract of A. sativum L.

2.3. Synthesis of ZnS NPs

In $ZnCl_2$ (5mM) solution, solution of Na_2S (5mM) was added drop with continuous stirring. While a white solution was formed, *A. sativum L.* extract was added drop wise.

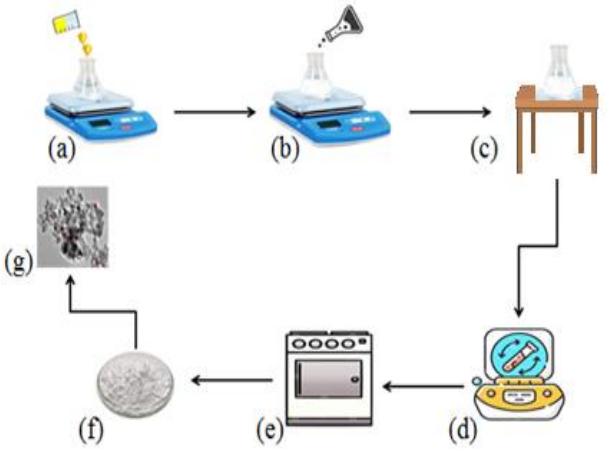

Fig. 2. (a) Drop wise addition of Na_2S solution in $ZnCl_2$, (b) drop wise addition of A. sativum L. extract in ($ZnCl_2$ + Na_2S) solution with continuous stirring, (c) cloudy white precipitate, (d) centrifuged at 2,000 rpm, (e) dried at 70^0 C in oven, (f) ZnS powder sample and (g) ZnS NPs.

The resultant solution was stirred for 2 hours and then kept for another one hour at room temperature without stirring to complete the reaction. A cloudy white precipitate was formed which indicated the formation of ZnS NPs. The precipitate was centrifuged for 20 minutes at 2,000 rpm. The final product was dried at 70^0 C for 6 hours. Then it was crushed to fine powder. This process was carried out for 10 ml, 20 ml and 30 ml of *A. sativum L.* extract in order to get three

varieties samples. These samples were labeled as I, II and III respectively. The schematic diagram of preparation of ZnS NPs is shown in Fig.2

2.4. Characterization techniques

X-ray diffraction (XRD) patterns were recorded using an X-ray diffractrometer (Philips X' pert with CuK_{α} radiation) of wavelength 0.154 nm. SEM images were obtained using JEOL, JAPAN-JSM-6360. TEM micrographs were obtained in JEOL JEM 2100 using an accelerating voltage of 200 KV. EDAX (Oxford, INCA-7587) was used for elemental analysis of the samples. UV-Visible spectra were recorded in a Hitachi U-3210 spectrometer and FTIR spectra were recorded by Perkin Elmer spectrum RXI FTIR system. Dielectric, impedance and a.c. conductivity were recorded using LCR Hitester HIOKI 3532.D.C. conductivity was recorded with the help of Keithley sourcemeter (mode 2400).

3. Results and discussions

3.1. XRD Study

Figure 3 Shows the XRD patterns of ZnS samples prepared by using three different amounts of *A. sativum L.* extract. For the sample I, three broad peaks are observed in the diffractrogram at around 28.75^{o}, 47.93^{o}, 56.50^{o}. These peaks respectively correspond to (111), (220) and (311) planes of cubic ZnS [13]. It is found that for sample II and III there is a slight shift in the peak positions along with an increase in peak broadening. These broad peaks imply the presence of smaller particles. The crystallite size of the samples is calculated using Debye-Scherrer formula [14]

$$D = \frac{K\lambda}{\beta Cos\theta} \tag{1}$$

where D is the crystallite size, K is the geometric factor (0.98), λ is the X-ray wave length ($1.54A^{o}$), β is the full with at half maxima (FWHM) of the diffraction peak (in radian) and θ is the diffraction angles. The average crystallite size of the samples is found to be in the range 22.5 – 5.2 nm. The d-spacing and lattice constant 'a' for cubic phase ZnS structure are calculated using respectively the following relations [15, 16]

$$d_{hkl} = \frac{n\lambda}{2Sin\theta} \tag{2}$$

and

$$\frac{1}{d^2} = \frac{(h^2+k^2+l^2)}{a^2} \tag{3}$$

where h, k and l are Miller indices for the particular plane. The calculated lattice constants are found to be different for different orientation of the same sample which is because of the divergence of the X-ray beams, refraction and absorption of X-rays by the specimens etc. It is also found that the lattice constant of the samples is smaller than that of the bulk ZnS (a = 5.406 A^{0}, JCPDS: 050566). This is due to the presence of strain in the samples. The average strain (ε_{Strain}) of the samples is estimated using Stokes-Wilson equation [17]

$$\mathcal{E}_{\text{Strain}} = \frac{\beta}{4tan\theta} \tag{4}$$

where β is the FWHM and θ is the diffraction angle.

Since the strain is related to the dislocation produced in the crystal and dislocation represents the amount of defects present in the samples, the dislocation density (δ) of the samples is estimated using the Williamson-Smallman formula [17]

$$\delta = \frac{1}{D^2} \quad (5)$$

where D is the average crystallite size.

Table 1 shows the structural parameters. From table 1 it is found that as the volume of the *A. sativum L.* extract increases, the crystallite size of the ZnS NPs decreases. It is also found that dislocation density and average strain increases with decrease in crystallite size. Bilgin et al. [18] reported that higher values of dislocation density leads to the increase in the concentration of lattice imperfection. Therefore, in the present case, the decrease of crystallite size is associated with the incorporate of more defects in the crystals.

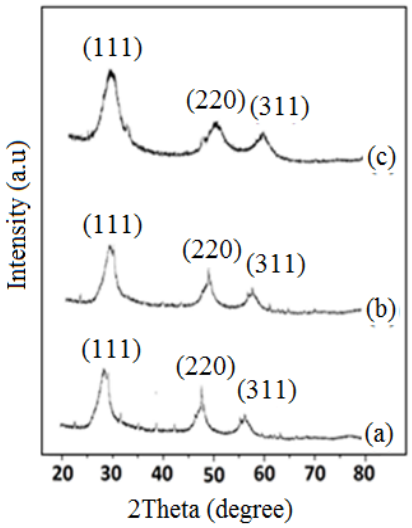

Fig. 3. XRD pattern of (a) sample I, (b) sample II and (c) sample III.

Table 1. Structural parameters of ZnS NPs.

Sample	2θ(degree)	FWHM(rad)	D(nm)	hkl	d(A°)	a(A°)	$\varepsilon_{Strain} x 10^{-3}$	$\delta(x10^{15})$ lines/m^2
I	28.75 47.93 56.50	0.00271 0.02906 0.03418	22.5	(111) (220) (311)	3.11 1.89 1.62	5.39 5.37 5.39	2.6	1.97
II	28.54 47.93 56.70	0.00323 0.03135 0.03157	19.5	(111) (220) (311)	3.14 1.89 1.62	5.45 5.36 5.38	3.1	2.62
III	28.32 47.73 56.50	0.04443 0.02369 0.03157	5.2	(111) (220) (311)	3.16 1.90 1.62	5.49 5.39 5.39	44.0	3.69

3.2. EDAX study

Figure 4 shows EDAX spectrum of one representative sample. EDAX spectrum confirms the presence of Zn and S and hence the formation of ZnS. In addition to Zn and S, there are elemental signals for C and O which might have come from proteins or enzymes present in the *A. sativum L.* extract [9, 17]. The inset of Fig.4 shows the atomic percentage of the compositional

elements. It is found that the measured S/Zn ratio is lower than the theoretical stoichiometry. This indicates the presence of sulphur vacancy in the sample [1].

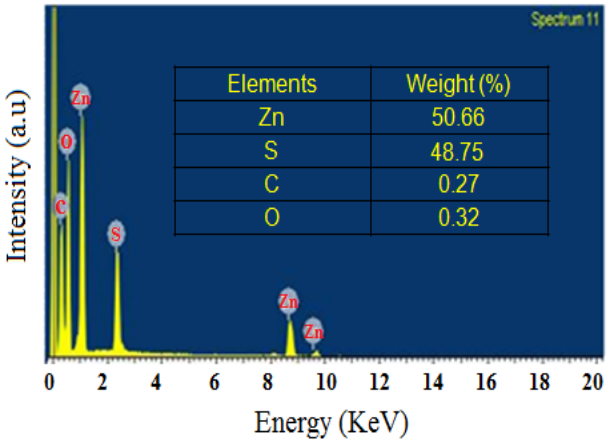

Fig. 4. EDAX spectrum of sample III. Inset shows the atomic percentage of compositional elements.

3.3. TEM and HRTEM analysis

Figure 5 shows the TEM image of one representative sample (sample III), which demonstrates the presence of a large number of spherical ZnS NPs. The average size of the NPs is found to be 6.5 nm, which is very close to the result obtained from XRD. Figures 5(b) and 5(c) respectively show the HRTEM image and SAED pattern of the sample. SAED pattern shows three diffraction rings which correspond to (111), (220) and (311) planes. This is in agreement with the XRD result. The HRTEM image shows lattice fringes with adjacent plane spacing of 0.31nm, which correspond to (111) plane of cubic ZnS.

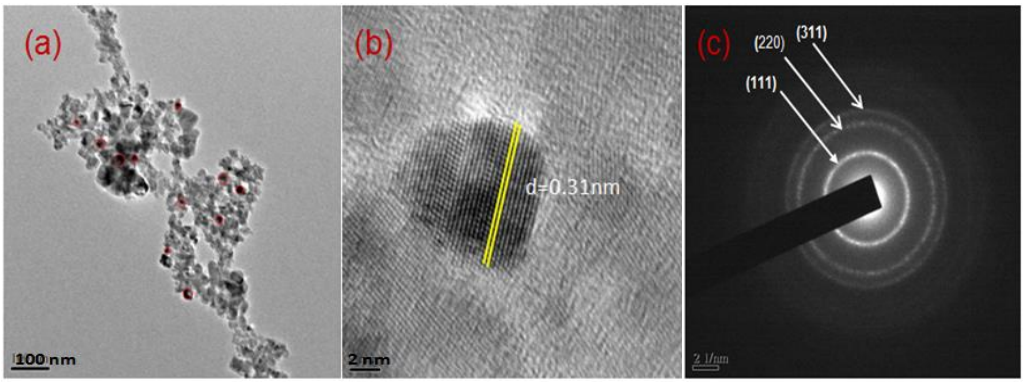

Fig. 5. (a) TEM image of ZnS NPs, (b) HRTEM image and (c) SAED pattern.

3.4. UV-Visible study

Figure 6 (a) shows the UV-Visible absorption spectra of samples I, II and III. It is found that absorption peaks are blue shifted and their intensities are also very strong. This type of strong intensity peak appears due to quantum confinement effect [19]. For direct allowed transition, the incident photon energy ($h\nu$) and absorption coefficient (α) can be related by the following Tauc's equation [20]

$$(\alpha h\nu)^{\frac{1}{2}} = A(h\nu - E_g) \tag{6}$$

where A is a constant and E_g is the direct band gap energy. The direct band gap energy of the samples is calculated by plotting $(\alpha h\nu)^2$ versus $h\nu$ and extrapolating the linear portion of the curve on $h\nu$ axes to $\alpha = 0$. The calculated direct band gap energy is found to increase from 3.87 – 4.25 eV with increasing volume of the *A. sativum L.* extract. It is seen that these band gap values are higher compared to the band gap value of bulk ZnS which demonstrates the presence of nanoparticles in the samples. The variation of the band gap is due the existence of the trapping levels whose discrete energies are located within the band gap [21]. The trapping levels typically possess dipole moments considerably larger than that of the bulk materials [21]. Since the physical properties of an optical material depend on the dimension of the material [22], the particle size (in nm) of the samples is calculated using the formula [23]

$$d(E) = \frac{0.32 - 2.9\sqrt{E - 3.49}}{3.50 - E} \tag{7}$$

The calculated particle size is found to be in the range 3.9 – 2.9 nm. The particle size determined by TEM and UV–Vis spectroscopy is found to be different. This could be because UV–Vis spectroscopy is only sensitive to the crystalline core size and identifies defect-free domain sizes, whereas the size from TEM can be larger if inner aggregate interfaces are not recognized. It is known that the refractive index (n) of optical materials is very essential to design heterostructure lasers in optoelectronic devices along with solar cell applications. Therefore, refractive index of the samples is calculated using the formula [24]

$$E_g n^4 = 95\ eV \tag{8}$$

where E_g is the band gap energy. The calculated refractive index is found to vary from 2.23 – 2.17 for samples I – III respectively. This type of high refractive index optical materials is suitable for applications in lenses, prism, waveguide and light-emitting diodes [25-27].

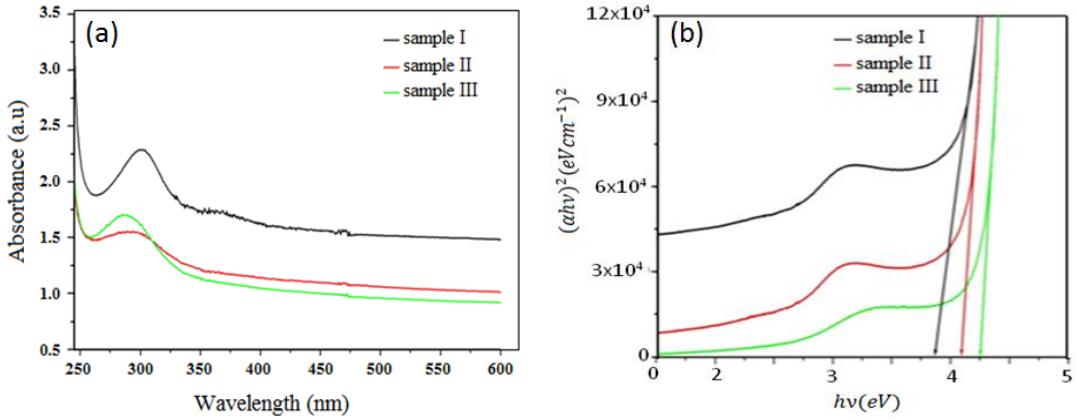

Fig. 6. (a) Absorption spectra of the ZnS samples and (b) Tauc's plot of the samples.

3.5. FTIR Study

As FTIR has been proven to be an important characterization tool for the identification of compounds or functional groups [28], in the present study FTIR of one representative sample (sample III) has been carried out (Fig.7) to identify the possible functional groups of biomolecules responsible for stabilizing and capping of ZnS NPs. The FTIR spectrum of the synthesized ZnS NPs shows peaks at 3360 cm^{-1}, 1633 cm^{-1} and 1012 cm^{-1} corresponding to N-H and O-H (stretching mode in the linkage of proteins), C = O (stretching mode in amide-I group of protein) and C–N (stretching in the primary amines) respectively [29-32]. All these functional groups are also present in pure *A. sativum L.* extract which was confirmed by Yulizar et al. [32] through FTIR analysis. Therefore, it could be attributed that these biomolecules present in *A. sativum L.* extract

are responsible for capping and stabilization of ZnS NPs. Similar observation from FTIR study of ZnS NPs synthesized by using plant extracts such as *Elaeocarpus floribundus* [9], *Stevia rebaudiana Bertoni* [10] and *Azadirachta indica* [2] have been reported.

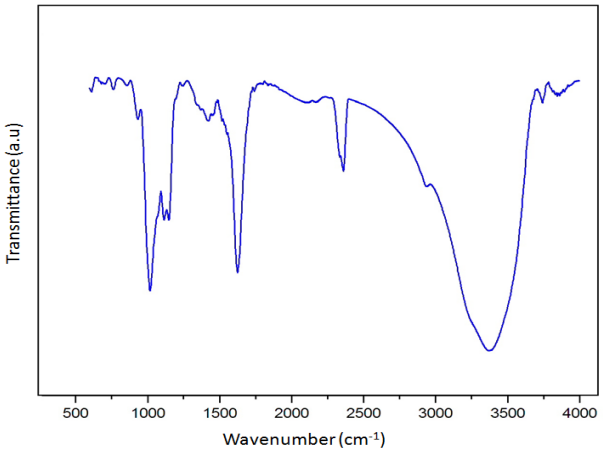

Fig. 7. FTIR spectrum of ZnS NPs.

3.6. Possible Growth Mechanism

The exact mechanism of the formation of ZnS NPs by the plant extract is not yet clearly understood. However, the possible growth mechanism may be explained as- (i) firstly, the cyclic structure of protein binds the ZnS cluster to its core and is thus stabilized in situ by the amide group of the peptide. As a result, ZnS NPs with a radius comparable to that of the cyclic peptide cavity is formed (ii) the stabilized ZnS NPs are later encapsulated by carboxyl compounds and other biomolecules contained in the extract because of their shape directing ability. The possible growth mechanism is depicted in Figure 8.

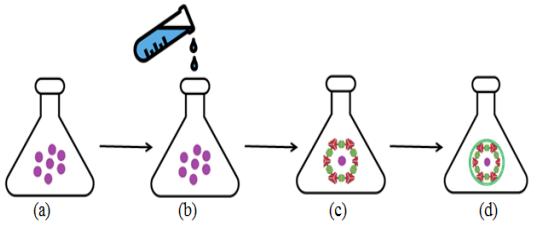

Fig. 8. Possible growth mechanism (a) ZnS clusters in the medium, (b) addition of A. sativum L. extract to the ZnS clusters (c) protein-ZnS electrostatic interaction: stabilization and (d) stabilized ZnS NPs are capped by the biomolecules.

3.7. Dielectric Properties

The dielectric is considered as the most important component of a capacitor and capacitor is extensively used to design different types of electronic circuits. The dielectric constant is the measure of the capability of the storing and transferring the electric charge and is one of the essential properties of a dielectric material. In this line, the dielectric constants of the synthesized samples are calculated using the relation [33]

$$\varepsilon' = \frac{Cd}{\varepsilon_o A} \tag{9}$$

where, C denotes capacitance, d denotes thickness, A denotes area of the sample and ε_o denotes absolute permittivity of free space. Figure 9 illustrates the dielectric constant of the samples as a function of frequency at room temperature. From this figure, it is observed that the dielectric

constant of the samples decreases exponentially with increasing frequency and then attains a constant value in the higher frequency region. It is known that the total polarization of a material is due to the contribution of electronic, ionic, orientations and interfacial polarizations [33]. The exponential decrease of dielectric constant in the present case is due to the effect of reduction of space charge polarization and constant values of dielectric constant in the higher frequency region are because of the interfacial polarization [34]. The dielectric constant of the samples is found to be higher in the lower frequency range. This is due to the reason that at the grain boundaries there exists space charge polarization that generates a potential barrier. As a result, charges are accumulated at the grain boundary and hence the higher values of dielectric constant. It is seen that dielectric constant are increasing with increasing the volume of the *A. sativum L.* extract. This may be due to the fact that the increase of the extract volume is associated with the increment of the concentration of the biopolymers during the preparation of the ZnS NPs along with the presence of crystal defects, contribute to have more polar centers on the structure and hence increasing the dielectric constant. Furthermore, the value of the dielectric constant of the ZnS NPs (particularly for the samples II and III) is higher compared to the dielectric constant value of bulk ZnS (8.3) [35]. This can be explained as follows: when an electric field is applied to ZnS samples, the positive and negative charges of the interfaces shift towards the applied field's negative and positive poles, respectively. Concurrently, large numbers of dipole moments are formed after they have been trapped by the defects. Because of this, space-charge polarization arises at the interface of the ZnS NPs which is the cause of much higher value of dielectric constant of the ZnS NPs. The findings of the dielectric characterization of the present work are the important parameters of materials essential for ferroelectric, photonic and electronic devices.

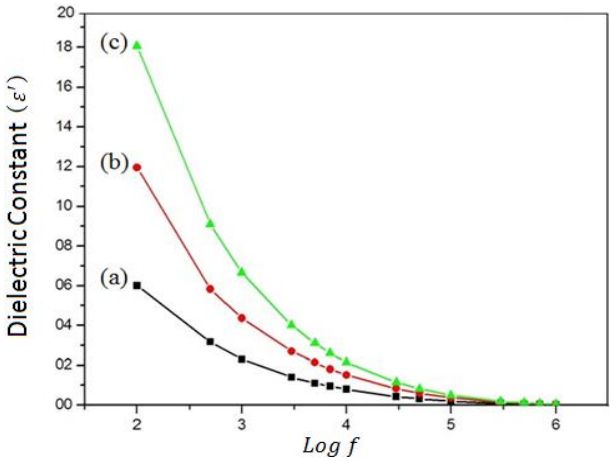

Fig. 9. Variation of dielectric constant with frequency of the samples.

3.8. A.C conductivity

A.C. conductivity gives the information about the charge carriers involved in the conduction process. The A.C conductivity of the prepared samples are calculated using the formula [33]

$$\sigma_{ac} = 2\pi f \varepsilon_o \varepsilon_r tan\delta \tag{10}$$

where, f, ε_o , ε_r and $tan\delta$ respectively represent frequency, permittivity of free space, dielectric constant and dielectric loss factor respectively. Figure 10 depicts the A.C. conductivity of the samples as a function of frequency. The A.C. conductivity increases with increasing frequency, as shown in this graph. The pumping force of the applied field induces the transfer of charge carriers between distinct localised states as well as the liberation of trapped charges from different trapping centres, resulting in an increase in A.C. conductivity. The conduction process is aided by these mobile charge carriers [36].

According to Jonscher's power law [37], A.C. conductivity is given by

$$\sigma_{ac}(\omega) = \sigma_{dc} + A\omega^{S} \quad (11)$$

where, σ_{dc} is the d.c conductivity of the material at low frequency, A is a constant, ω is angular frequency and S is the frequency exponent. The variation of the frequency exponent 'S' with temperature can be utilized to determine the material's conduction process. Therefore, the values of 'S' computed (for one representative sample III) by fitting conductivity data with $\sigma_{ac}(\omega) = A\omega^{S}$ are plotted as a function of temperature and is shown in the inset of figure10. There are numerous models that explain the conduction process of the materials depending on the value and behaviour of 'S'. In quantum tunneling model (QTM), 'S' depends on frequency but independent of temperature [38]. In small polaron tunneling model (SPT), 'S' increases with increasing temperature [39]. In large polaron tunneling model (LPT), 'S' depends on temperature as well as frequency [40]. In correlated barrier-hopping model (CBH), 'S' decreases with increasing temperature [41]. The plot of 'S' vs. temperature (inset of Fig.10) shows that 'S' decreases with increasing temperature. Therefore, the A.C. conduction in nanostructured ZnS obeys CBH model.

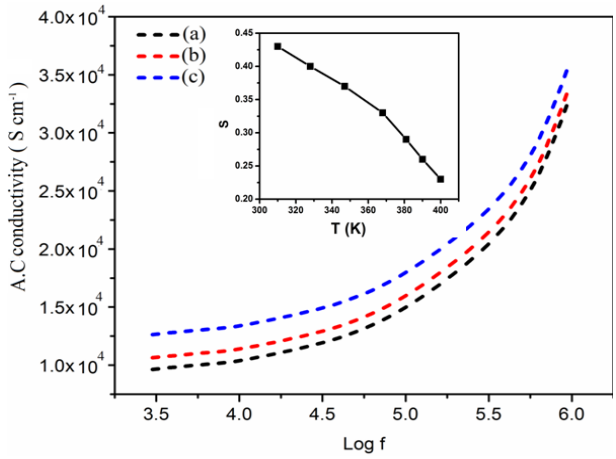

Fig. 10. Plot of A.C conductivity vs frequency of (a) sample I, (b) sample II and (c) sample III. Inset shows frequency exponent 'S' as a function of temperature of sample III.

3.9. Impedance Study

Figure 11 shows the variation of admittance of ZnS samples with frequency. From this figure, it is seen that admittance grows rapidly until it reaches a particular frequency known as the resonance frequency, after which it drops. This type of variation of admittance with applied frequency exhibits the capacitance impedance involved with the nano materials [42]. The steep rise and fall of admittance at a specific frequency is the property of electronic tuned circuit. The frequency at which the maximum admittance is achieved can be compared to the resonance frequency of a typical tuned circuit, and this frequency is referred to as the "equivalent resonant frequency." [43]. S. S. Nath et al. [44] reported that bulk ZnS does not show any variation in admittance with frequency. Therefore, the synthesized ZnS nanomaterials can be used in nano-tuned devices.

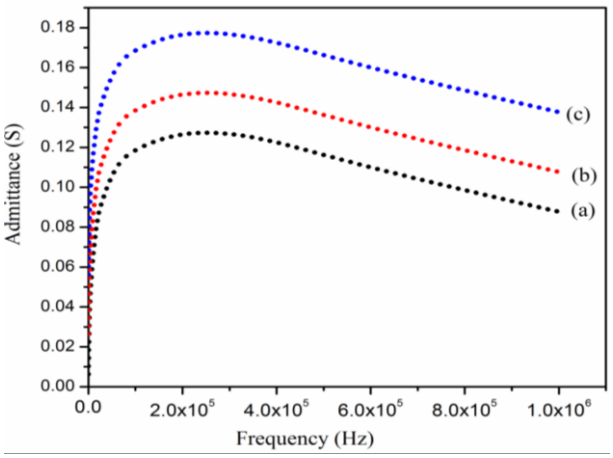

Fig. 11. Variation of admittance of (a) sample I, (b) sample II and (c) sample III with frequency.

3.10. D.C conductivity

Figure 12 shows the variation in σ_{dc} of ZnS NPs with average crystallite size of 22.5, 19.5 and 5.2 nm in the temperature range of 285K – 400K. It can be seen in this figure that σ_{dc} increases with increase in temperature and decrease in average crystallite size. For NPs of various average crystallite sizes, the nature of variation in $\sigma_{dc}$with temperature is comparable. The σ_{dc} of ZnS NPs is found to be on the order of $10^{-11}\ \Omega^{-1}\ cm^{-1}$, which is greater than the bulk ZnS ($10^{-13}\ \Omega^{-1}\ cm^{-1}$) [45]. Thermionic emission is the most common charge transfer mechanism across the grain boundary barrier in polycrystalline semiconductors [46]. According to previous research, thermionic emission is the dominant electrical transport mechanism when a material's conductivity exhibits Arrhenius behavior [47]. Figure 12 show that the ZnS samples have a temperature dependence of σ_{dc} that is roughly Arrhenius type. As a result, it is plausible to believe that the predominant electrical transport mechanism in ZnS NPs is thermionic emission of charge carriers over barriers. The function of deep and shallow trap states in carrier transport through grain boundaries in semiconductors was elucidated by Blatter et al [48]. Deep trap states are spatially localised and are found deep at the band edge, whereas shallow trap states are found within 3-5 meV of the band edge. The shallow trap responds to a tiny size before the deep traps as grain size declines. Deep trap states, on the other hand, are so far within the gap that trapped charge carriers cannot be easily thermally ionised [49]. Therefore, for ZnS NPs, it can be hypothesised that as temperature rises, the likelihood of more charge carriers being caught in shallow trap states rises, lowering the grain boundary barrier height and making thermionic emission of charge carriers from one grain to another simpler, increasing σ_{dc}. The combined effect of grain boundaries and triple junctions inherent in nanostructured materials can explain the increase in σ_{dc} with decreasing average crystallite size [50]. Triple junctions, like grain boundaries, are significant components of the interface [51, 52]. They are the intersection lines of three or more neighboring grains. For computing interfacial volume percentage, nanostructure materials' grains are considered to have a regular tetrakaidecahedron shape, with hexagonal faces representing grain boundaries and edges corresponding to triple junctions [52]. By assuming that grains have a normal tetrakaidecahedron structure, volume fractions of the entire interfacial region (V_{if}), grain boundaries (V_{gb}), and triple junction (V_{tj}) are estimated in this study. The volume fractions are given by [53]

$$V_{if} = 1 - [(D-d)/D]^3 \tag{12}$$

$$V_{gb} = [3d(D-d)^2]/D^3 \tag{13}$$

$$V_{tj} = [\,V_{if} - V_{gb}\,] \tag{14}$$

where D is the average crystallite size and d/2 is the interfacial area thickness [51, 52]. For all calculations, d/2 is set to 0.5 nm, which is a reasonable size for the samples utilised in this investigation [52].The variation of V_{if}, V_{gb} and V_{tj} with average crystallite size of ZnS NPs is shown in figure 13. According to this figure, V_{if} is largest for sample III with a minimal average crystallite size of 5.2 nm and steadily decreased as the average crystallite size increased to 22.5 nm for sample I. $V_{gb}$and V_{tj} values are also higher in smaller crystallites. That is, the volume fractions of the interfacial region, grain borders and triple junctions increase when the average crystallite size decreases, increasing the possibility of more charge carriers being trapped at shallow grain boundary level. As a result, the barrier height of grain boundaries reduces, making thermionic emission of charge carriers from one grain to another simpler. This leads to an increase in σ_{dc} as the average crystallite size of ZnS NPs decreases.

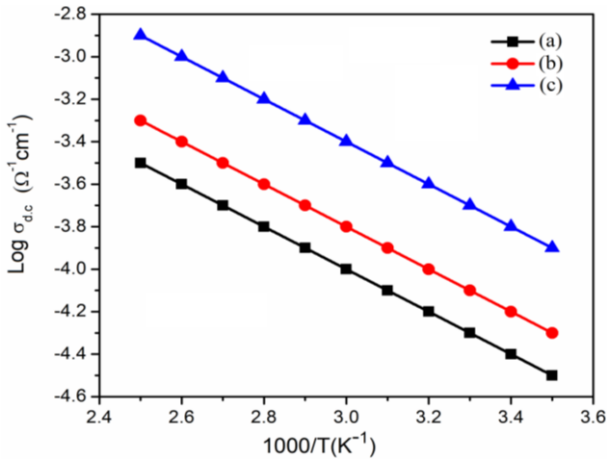

Fig. 12. Variation in σ_{dc} with temperature for (a) sample I, (b) sample II and (c) sample III.

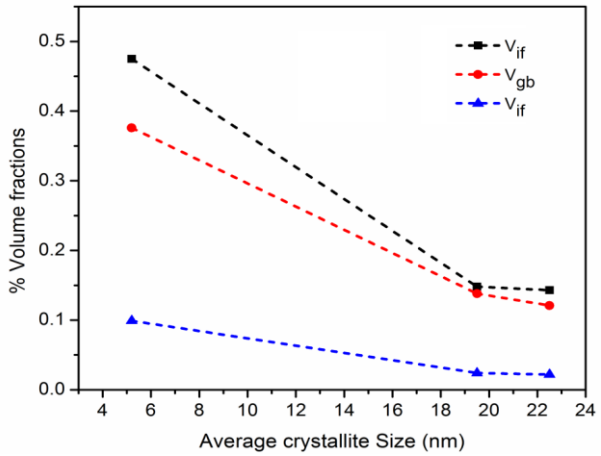

Fig. 13. Variation of volume fractions with average crystallite size of ZnS NPs.

4. Conclusions

A simple, economic and environmentally friendly route has been used for the synthesis of ZnS NPs. Extract of a locally available medicinal plant *Allium sativum L.* is used as stabilizing and capping agent for this synthesis purpose. XRD results show that the crystallite size of the ZnS NPs decreases from 22.5 – 5.2 nm as the volume of the extract is increased from 10 – 30 ml. This implies that the crystallite size of the NPs can be varied by changing the volume of the extract. EDAX study confirms the presence of sulphur vacancy in the crystal. TEM study confirms the

formation of spherical particles of size about 6.5 nm. From UV-Visible study it is found that the direct band gap energy of the nanopartcles increases from 3.87 – 4.25 eV with increasing volume of the extract. The refractive index of the NPs is found to vary from 2.23 – 2.17. FTIR study confirms the presence of protein in the extract. A possible growth mechanism is suggested in which it is believed that ZnS NPs are stabilized in situ by the amide group of the peptide and capped by the carboxyl compound and other such biomolecules present in the extract due to their shape directional ability. Exponential decreases of the dielectric constant with increasing frequency along with constant value in the higher frequency region of the samples are observed. The observed dielectric parameters of the synthesized NPs are suitable for fabrication of materials required for electro-optical devices. In the higher frequency range, A.C conductivity increases with increasing frequency and varies almost linearly with applied frequency. The correlated barrier-hopping model governs A.C conduction in ZnS NPs. The capacitive impedance associated with ZnS nanoparticles is indicated by the variation of impedance with frequency. These materials have the potential to be employed in electronic nanotuned devices. The ZnS NPs have a greater σ_{dc} than bulk ZnS. The thermionic emission of charge carriers causes the increase in σ_{dc}. To explain the variation of σ_{dc} with average crystallite size, the combined effect of grain boundaries and triple junctions on electrical transport is considered.

Acknowledgements

The author acknowledges institutional biotech bub, Handique Girls' College, Guwahati for providing laboratory facilities and SAIF (NEHU), Shillong, and IIT Guwahati for providing characterization facilities.

References

[1] J. Koaib, N. Bouguila, H. Abassi, N. Moutia, M. Kraini, A. Timoumi, C. Vazquez-Vazquez, K. Khirouni, S. Alaya, RSC Adv. **10**, 9549 (2020); https://doi.org/10.1039/C9RA10284A
[2] S. C. Tudu, M. Zubko, J. Kusz, A. Bhattacharjee, Int. J. Nano Dimens. **11**, 99 (2020).
[3] B. Vaidhyanathan, M. Ganguli, K. J. Rao, Mater. Res. Bull. **30**, 1175 (1995); https://doi.org/10.1016/0025-5408(95)00099-2
[4] L. M. Qi, J. M. Ma, H. M. Cheng, Z. G. Zhao, J. Colloids Surf. A **111**, 195 (1996); https://doi.org/10.1016/0927-7757(96)03545-5
[5] V. Bessergenev, E. N. Ivanova, Yu. A. Kovalevskaya, S. A. Gromilov, V. N. Kirichenko, S. M. Zemskova, I. G. Vasilieva, B. M. Ayupov, N. L. Shwarz, Mater. Res. Bull. **30**, 1393 (1995); https://doi.org/10.1016/0025-5408(95)00150-6
[6] J. Liu, J. Ma, Z. Y. Liu, Y. Song, J. Sun, Z. L. Fang, J. Alloys Comp. **486**, 40 (2009); https://doi.org/10.1016/j.jallcom.2009.07.109
[7] Y. Y. She, J. Yang, K. Q. Qiu, Trans. Nanferrous Met. Soc. **20**, 211 (2010); https://doi.org/10.1016/S1003-6326(10)60041-6
[8] S. H. Ansari, F. Islam, M. Sameem, J. Adv. Pharm Technol Res. **3**, 142 (2012); https://doi.org/10.4103/2231-4040.101006
[9] U. S. Senapati, D. Sarkar, J.Mater.Sci: Mater Electron. **26**, 5783 (2015); https://doi.org/10.1007/s10854-015-3137-6
[10] H. Q. Alijani, S. Pourseyedi, M. T. Mahani, M. Khatami, J. Molecular Struct. **1175**, 214 (2019); https://doi.org/10.1016/j.molstruc.2018.07.103
[11] G. A. Otunola, A. J. Afolayan, E. O. Ajayi, S. W. Odeyemi, Phcog Mag. **13**, 201 (2017); https://doi.org/10.4103/pm.pm_430_16
[12] M. Ali, M. Ikram, M. Ijaz, A. Ul-Hamid, M. Avais, A. A. Anjum, Appl. Nanosci. **10**, 3787 (2020); https://doi.org/10.1007/s13204-020-01451-6
[13] R. Sahraei, G. M. Aval, A. Baghizadeh, M. L. Rachi, A. Goudarzi, M. H. Majlesara, Mater. Lett. **62**, 4345 (2008); https://doi.org/10.1016/j.matlet.2008.07.022

[14] K. A. Salman, K. Omar, Z. Hassan, Superlatti. Micro Struct. **50**, 647 (2011); https://doi.org/10.1016/j.spmi.2011.09.006
[15] M. Dhanam, B. Kavitha, S. Velumani, Mat. Sci. Eng. B **174**, 209 (2010); https://doi.org/10.1016/j.mseb.2010.03.028
[16] R. Kripal, A. G. Gupta, S. K. Mishra, R. K. Srivastava, A. C. Pandey, S. G. Prakash, Spectrochim Acta Part A **76**, 523 (2010); https://doi.org/10.1016/j.saa.2010.04.018
[17] U. S. Senapati, D. Sarkar, Indian J. Phys. **88**, 557 (2014); https://doi.org/10.1007/s12648-014-0456-z
[18] V. Bilgin, S. Kose, F. Atay, I. Akyuz, Mater. Chem. Phys. **94**, 103 (2005); https://doi.org/10.1016/j.matchemphys.2005.04.028
[19] W. Vogel, P. H. Borse, N. Deshmukh, S. K. Kulkarni, Langmuir **16**, 2032 (2000); https://doi.org/10.1021/la9910071
[20] C. S. Pathak, M. K. Mandal, V. Agarwala, Superlattices Microstruct. **58**, 135 (2013); https://doi.org/10.1016/j.spmi.2013.03.011
[21] I. V. Kityk, J. Non-Cryst. Sol. **292**, 184 (2001); https://doi.org/10.1016/S0022-3093(01)00860-2
[22] T. M. Williams, D. Hunter, A. K. Pradhan, I. V. Kityk, Appl. Phys. Lett. **89**, 043116 (2006); https://doi.org/10.1063/1.2236211
[23] J. F. Suyver, S. F. Wuister, J. J. Kelly Meijerink, Nano Lett. **1**, 429 (2001); https://doi.org/10.1021/nl015551h
[24] N. M. Ravindra, P. Ganapathy, J. Choi, Infrared Phys. Technol. **50**, 21 (2007); https://doi.org/10.1016/j.infrared.2006.04.001
[25] C. Lu, B. Yang, Journal of Materials Chemistry **19**, 2884 (2009); https://doi.org/10.1039/b816254a
[26] F. W. Mont, J. K. Kim, M. F. Schubert, E. F. Schubert, R. W. Siegel, Journal of Applied Physics **103**, 083120 (2008); https://doi.org/10.1063/1.2903484
[27] J. Liu, M. Ueda, Journal of Materials Chemistry **19**, 8907 (2009); https://doi.org/10.1039/b909690f
[28] G. A. Otunola, A. J. Afolayan, E. O. Ajayi, S. W. Odeyemi, Phcog Mag **13**, 201 (2017); https://doi.org/10.4103/pm.pm_430_16
[29] Y. Y. Loo, B. W. Chieng, M. Nishibuchi, S. Radu, Int. J. Nanomed. **7**, 4263 (2012).
[30] S. Tajammul Hussain, M. Iqbal, M. Mazhar, J. Nanopart. Res. **11**, 1383 (2009); https://doi.org/10.1007/s11051-008-9525-6
[31] J. Huang, Q. Li, D. Sun, Y. Lu, Y. Su, X. Yang, H. Wang, Y. Wang, W. Shao, N. He, J. Hong, C. Chen, Nanotechnology **18**, 105104 (2007); https://doi.org/10.1088/0957-4484/18/10/105104
[32] Y. Yulizar, H. Atika Ariyanta, L. Abdurrachman, Bulletin of Chemical Research Engineering & Catalysis **18**, 212 (2017); https://doi.org/10.9767/bcrec.12.2.770.212-218
[33] S. Suresh, Appl. Nanosci. **4**, 325 (2014); https://doi.org/10.1007/s13204-013-0209-x
[34] Ch. Rayssi, S. El. Kossi, J. Dhahri, K. Khirouni, RSC Adv. **8**, 17139 (2018).
[35] I. Parvanesh, S. Samira, N. Mohsen, Chinese Physics B **24**, 046104 (2015); https://doi.org/10.1088/1674-1056/24/4/046104
[36] V. P. Singh, G. Kumar, P. Dhiman, R. K. Kotnala, J. Shah, K. M. Batto, M. Singh, Adv. Mater. Lett. **5**, 447 (2014); https://doi.org/10.5185/amlett.2014.554
[37] M. A. El Hiti, J. Phys. D Appl. Phys. **29**, 501 (1996); https://doi.org/10.1088/0022-3727/29/3/002
[38] A. Ghosh, Phys. Rev. B **42**, 5665 (1990); https://doi.org/10.1103/PhysRevB.42.566
[39] D. L. Tonks, R. N. Silver, Phys. Rev. B **26**, 6455 (1982), https://doi.org/10.1103/PhysRevB.26.6455
[40] A. Ghosh, Phys. Rev. B **42**, 1388 (1990); https://doi.org/10.1103/PhysRevB.42.1388
[41] G. E. Pike, Phys. Rev. B **6**, 1572 (1972); https://doi.org/10.1103/PhysRevB.6.1572
[42] A. Firdous, M. Aslam Baba, D. Singh, A. H. Bhat, Appl. Nanosci. **5**, 201 (2015); https://doi.org/10.1007/s13204-014-0306-5
[43] S. D. Bompilwar, S. B. Kondawar, V. A. Tabhane, Arch. Apll. Sci. Res. **2**, 225 (2010).
[44] S. S. Nath, D. Chakdar, G. Gopal, D. K. Avasthi, Azajonano-J., Nanotechnology **4**, 1(2008).

[45] E. Birringuier, Phil. Mag. B **75**, 209 (1997), https://doi.org/10.1023/A:1018959529628
[46] V. Snejdar, J. Jerhot, Thin Solid Films **37**, 303 (1976); https://doi.org/10.1016/0040-6090(76)90600-3
[47] Y. W. J. Setto, J. Appl. Phys. **46**, 5247 (1975); https://doi.org/10.1063/1.321593
[48] G. Blatter, F. Greuter, Phys. Rev. B **33**, 3952 (1986); https://doi.org/10.1103/PhysRevB.33.3952
[49] L. Brus, J. Phys. Chem. **90**, 2555 (1986); https://doi.org/10.1021/j100403a003
[50] V. Biju, M. A. Khadar, Mater. Res. Bull. **36**, 21 (2001), https://doi.org/10.1016/S0025-5408(01)00488-3
[51] C. Suryanarayana, Bull. Mater. Sci. **17**, 302 (1994), https://doi.org/10.1007/BF02747225
[52] G. Palumbo, S. J. Thorpe, K. T. Aust, Scr. Matall. Mater. **24**, 1347 (1990); https://doi.org/10.1016/0956-716X(90)90354-J
[53] S. S. Nair, M. A. Khadar, Sci. Technol. Adv. Mater. **9**, 035010 (2008); https://doi.org/10.1088/1468-6996/9/3/035010